Acyclic Immucillin Phosphonates: Second generation inhibitors of *Plasmodium falciparum* hypoxanthine-guanine-xanthine phosphoribosyltransferase

Keith Z. Hazleton[1], **Meng-Chiao Ho**[1], **Maria B. Cassera**[1,#], **Keith Clinch**[2], **Douglas R. Crump**[2], **Irving Rosario Jr.**[1], **Emilio F. Merino**[1,#], **Steve C. Almo**[1], **Peter C. Tyler**[2], and **Vern L. Schramm**[1,*]

[1]Department of Biochemistry, Albert Einstein College of Medicine, Yeshiva University, Bronx, New York 10461, USA [2]Carbohydrate Chemistry Group, Industrial Research Ltd., 69 Gracefield Road, Lower Hutt 5040, New Zealand

Summary

Plasmodium falciparum, the primary cause of deaths from malaria, is a purine auxotroph and relies on hypoxanthine salvage from the host purine pool. Purine starvation as an antimalarial target has been validated by inhibition of purine nucleoside phosphorylase. Hypoxanthine depletion kills *Plasmodium falciparum* in cell culture and in *Aotus* monkey infections. Hypoxanthine-guanine-xanthine phosphoribosyltransferase (HGXPRT) from *P. falciparum* is required for hypoxanthine salvage by forming inosine 5′-monophosphate, a branchpoint for all purine nucleotide synthesis in the parasite. Here we present a new class of HGXPRT inhibitors, the acyclic Immucillin phosphonates (AIPs), and cell permeable AIP prodrugs. The AIPs are simple, potent, selective and biologically stable inhibitors. The AIP prodrugs block proliferation of cultured parasites by inhibiting the incorporation of hypoxanthine into the parasite nucleotide pool and validates HGXPRT as a target in malaria.

Introduction

Malaria is a major global health concern that is responsible for greater than 200 million clinical cases and 800,000 deaths each year (WHO, 2008). The vaccines for malaria currently in clinical trials confer limited protection and resistance to artemisinin and its derivatives has been detected in Southeast Asia (Bejon et al., 2008; Noedl et al., 2008). These developments illustrate the continued need to develop new antimalarial compounds against novel targets.

Plasmodium falciparum lacks the enzymatic machinery to synthesize purines *de novo* (Reyes et al., 1982). Additionally, the parasite lacks adenosine kinase or adenine phosphoribosyltransferase activity and relies on the conversion of hypoxanthine to inosine 5′-monophosphate by hypoxanthine-guanine-xanthine phosphoribosyltransferase

*vern.schramm@einstein.yu.edu, phone: 718-430-2814, fax: 718-430-8565.
#Current address: Department of Biochemistry, Virginia Tech, Blacksburg, VA 24061

(*Pf*HGXPRT) as its primary source of purines (Cassera et al., 2008). Hypoxanthine depletion through either xanthine oxidase-mediated degradation or purine nucleoside phosphorylase (PNP) inhibition has been demonstrated to kill parasites in cell culture (Berman and Human, 1991; Kicska et al., 2002b). Inhibition of both parasite and host PNP kills *P. falciparum* in *Aotus* monkeys (Cassera et al., 2011).

The transition states of N-ribosyl transferases are usually characterized by ribocation character and low bond order to the purine ring and the attacking nucleophile. For example, orotate phosphoribosyltransferases (Tao et al., 1996; Zhang et al., 2009) and purine nucleoside phosphorylases (Kline and Schramm, 1993, 1995) share these properties. HGXPRTs have resisted transition state analysis because of kinetic commitment factors. We proposed a transition state structure for *Pf*HGXPRT based on the assumption of ribocation character at the transition state of this reaction (Fig. 1a) (Li et al., 1999). Immucillin-H 5′-phosphate (ImmHP) has been shown to be a 1 nM inhibitor of *Pf*HGXPRT (Li et al., 1999). However, phosphate monoesters are incompatible with biological activity. The phosphate charges make ImmHP impermeable to cells and the phosphate group is vulnerable to the action of phosphomonoesterases. Keough and colleagues demonstrated inhibition of *Pf*HGXPRT by acyclic nucleoside phosphonates (Keough et al., 2009). These compounds replace the labile phosphate with a biologically stable phosphonate.

In this work we present a new class of selective *Pf*HGXPRT inhibitors, the acyclic Immucillin phosphonates (AIPs). The AIPs attain the affinity of ImmHP for *Pf*HGXPRT while being biologically stable and synthetically accessible. Prodrug analogues of AIPs are active against cultured *P. falciparum* and inhibit hypoxanthine incorporation. The mechanism of inhibition has been revealed with crystal structures of *Pf*HGXPRT in complex with an AIP and magnesium pyrophosphate and with a substrate complex of hypoxanthine and magnesium pyrophosphate.

Results

Action of Immucilin-H 5′-Phosphate

ImmHP is a 1 nM inhibitor of recombinant *Pf*HGXPRT and human HGPRT. However, ImmHP lacks activity against cultured *P. falciparum* in the presence of hypoxanthine (data not shown). We synthesized a prodrug of ImmHP to overcome the cell permeability barrier created by the negative charges of the 5′-phosphate group (**1** in Figure 2a). Compound **1** demonstrated a 5.8 ± 1.2 μM half maximal inhibitory concentration (IC_{50}) in assays with parasites (Fig. 2b). However, metabolic labeling studies of erythrocytes with **1** showed inhibition of inosine conversion to hypoxanthine resulting from the dephosphorylation of **1** to Immucillin-H, a powerful inhibitor of PNP (Fig. 2c and d). Treatment of infected erythrocytes with **1** and analysis by UPLC/MS/MS revealed that **1** is permeable to cells, but that cellular metabolism rapidly removes the 5′-phosphate to form Immucillin-H (Table S1), a potent inhibitor of *P. falciparum* and human PNPs (Kicska et al., 2002a).

Acyclic Immucillin phosphonates are selective and potent inhibitors of *Pf*HGXPRT

We identified two potent inhibitors of *Pf*HGXPRT (Fig. 1b). Both compounds were designed to match the predicted transition state features of ImmHP, specifically the 9-deazahypoxanthine nucleobase, ribocationic nitrogen, and a phosphonate group.

Both compounds **2** and **3** are competitive inhibitors of *Pf*HGXPRT with K_i values of 10.6 and 0.65 nM, respectively (Fig. 1c). When tested against human HGPRT compounds **2** and **3** displayed lower affinities of 4940 and 385 nM. Thus, compounds **2** and **3** are respectively 466- and 592-fold more selective for the parasite enzyme than the human enzyme.

AIP prodrugs inhibit proliferation of *Plasmodium falciparum* in culture by inhibiting hypoxanthine metabolism

The free phosphonate inhibitors showed no activity against cultured parasites, consistent with a lack of membrane permeability. Prodrug **4** (Fig. 3a), the bis-pivalate of **2**, inhibited the growth of cultured parasites with an IC_{50} of 45 ± 6 μM (Fig. 3b). Metabolic labeling of erythrocytes with [^{3}H]hypoxanthine in the presence of 100 μM **4** revealed incorporation of radiolabel into extracellular inosine and other intermediates and labeling with [^{3}H]inosine showed inhibition of inosine conversion to hypoxanthine (Fig. 3c). UPLC/MS/MS analysis of infected erythrocytes treated with 100 and 200 μM of **4** for 30 minutes confirmed that **4** is processed to **2** in infected erythrocytes, causing an increase in inosine concentration (Table S1). Hypoxanthine was not found in treated or control samples, suggesting that HG(X)PRT activity was unaffected. **2** inhibits human PNP with submicromolar affinity (Table S2). The accumulation of extracellular inosine from labeled erythrocytes indicates that **4** is permeable, but is converted to **2** before crossing the parasite membranes. In the erythrocyte, compound **2** inhibits PNP causing accumulation of inosine. At higher concentrations, **4** also crosses the parasite membranes, is activated and inhibits *Pf*HGXPRT activity.

Compounds **5, 6, 7** and **8** are lysophospholipid mimics intended to provide prodrug bioavailability (Fig. 4) (Hostetler, 2009). The prodrugs were assayed to determine the IC_{50} values against *P. falciparum* strain 3D7 (Fig. 4b). Compounds **5, 6** and **7** inhibited parasite growth *in vitro* with IC_{50} values of 2.5 ± 0.2 μM, 1.9 ± 0.1 μM, and 7.0 ± 0.1 μM, respectively. The IC_{50} values for compounds **5** and **6** were similar when tested against chloroquine/mefloquine-resistant strain Dd2 (3.0 ± 0.1 μM and 2.3 ± 0.1 μM) or chloroquine/quinine resistant strain FVO (2.9 ± 0.1 μM and 3.1 ± 0.1 μM). Compound **8** did not inhibit parasite growth at concentrations up to 15 μM. Parasite killing by inhibition of PNP can be rescued by exogenous hypoxanthine, but inhibition at *Pf*HGXPRT cannot (Kicska et al., 2002b). The IC_{50} assays were conducted at a range of exogenous hypoxanthine concentrations from 0 to 185 μM. The IC_{50} values showed no significant variation with increasing concentrations of exogenous hypoxanthine (all IC_{50} values between 2.2 and 2.4 μM from 3 to 185 μM hypoxanthine). Thus the site of action is inhibition of *Pf*HGXPRT (Fig. 4c).

We further defined *Pf*HGXPRT as the target of the AIP prodrugs by metabolic studies. Incorporation of radiolabeled hypoxanthine by uninfected erythrocytes was unchanged by incubation with 10 μM of **5** (Fig. 5a and Table 1). The label was incorporated into the erythrocyte IMP and GMP pools with smaller amounts appearing in GDP and GTP. The lack of incorporation into the adenine nucleotides is expected since human erythrocytes lack adenylosuccinate synthase activity. The effects of **5** on erythrocyte-free parasites consistently demonstrated a modest reduction of incorporation of hypoxanthine into the parasite nucleotide pool (Fig. 5b and Table 1).

The strongest effects of AIP inhibitors on *Pf*HGXPRT activity were seen in infected erythrocytes. Compounds **5** and **6** decreased incorporation of radiolabeled hypoxanthine by 85% (Figs. 5c, S1a and Table 1) and caused the accumulation of extracellular hypoxanthine (Fig. 5d). Inhibition was similar when **5** or **6** were present during incubation of parasites with radiolabeled hypoxanthine or in preincubation experiments where excess inhibitor was removed prior to the addition of radiolabel. Inhibition of hypoxanthine uptake by **5** or **6** was stronger in infected erythrocytes than in isolated parasites. Thus, erythrocytes play a role in activating the prodrug and/or transporting it into the parasite.

Compound **7** is the monoester of **5** and showed similar antiparasitic activity in IC_{50} assays (7.0 μM vs. 2.5 μM from Fig. 4c). In metabolic labeling experiments, incubation of infected erythrocytes with 15 μM **7** did not inhibit incorporation of label into parasitic nucleotides

(Fig. S1b). Thus, the ethyl phosphonate esters of **5** and **6** permit more effective inhibition of *Pf*HGXPRT than **7**.

In time- and concentration-dependent inhibition experiments, maximum inhibition of hypoxanthine uptake by **5** was complete after thirty minutes of treatment and increased linearly with concentrations of **5** between 0.5 and 5 µM (Figs. 5e and f).

Structural basis of inhibitor binding

Active site of PfHGXPRT—*Pf*HGXPRT forms a homotetramer in solution and each subunit is folded into a single domain containing the PRTase-like fold. Each subunit of the tetramer contains an active site, which can be divided into four functional regions: the purine binding site, the ribose binding site, 5′-phosphate binding site and pyrophosphate/magnesium ion binding site (Fig. 6). The purine-binding site is formed primarily by hydrophobic residues, including Tyr116, Ile146, Phe197, Val198 and Leu203 (Fig. 6a). Two charged residues in the purine-binding site, Asp146 and Lys176, form hydrogen bonds to N7 and O6 of the purine moiety of the inhibitors, respectively. The amide and carbonyl of Val198 and a water molecule, coordinated by a magnesium ion, form hydrogen bonds to O6, N1 and N3 of the purine, respectively. The ribose moiety interacts with magnesium pyrophosphate complex and Asp145 (Fig. 6b). The 5′-phosphate binding site is lined with the side chain residues of Tyr116, Thr149 and Thr152 and the amide nitrogens of Asp148, Thr149, Gly150 and Thr152 (Fig. 6c). Pyrophosphate is coordinated by the side chains of Arg112, Arg210, the amide nitrogens of Lys77, Gly78, Ser115 and Tyr116, and the magnesium ion (Fig. 6b). In the complex of ImmHP bound to *Pf*HGXPRT (PDB ID: 1CJB), the pyrophosphate ion-pairs with two magnesium ions, both octahedrally coordinated. One magnesium contacts O6 and O7 of the pyrophosphate, the side chain of Asp204 and three water molecules, while the second magnesium makes contact with O2 and O4 of the pyrophosphate, the 2′- and 3′-hydroxyls of ImmHP, and two water molecules. The first magnesium is conserved in *Pf*HGXPRT complexes with magnesium pyrophosphate and hypoxanthine and **3**. The second magnesium is absent in the complex with **3** and the first magnesium moves closer to the phosphate-binding site in the complex with hypoxanthine (Figs. 6b and S2a).

Binding of 3 to PfHGXPRT—The acyclic amino alcohol phosphonate is arranged in the active site of *Pf*HGXPRT to place the cationic amino group near the position occupied by the ribooxacarbenium ion in the proposed transition state. This positions the cation close to the pyrophosphate (2.8 Å; all distances are the average value from four monomers) to create a favorable ion pair. The methylene bridge linking the amino cation and 9-deazahypoxanthine allows the deazapurine to tilt 11° toward Phe197, a residue involved in aromatic ring stacking (Fig. 6d). The side chains of Asp148 (2.8 Å) and Lys (3.0 Å), the amide and carbonyl of Val (3.1 Å and 2.7 Å) and a structural water (2.6 Å) coordinated by magnesium are in hydrogen bonds with N7, O6, O6, N1 and N3 of the deazapurine of **3**, respectively. The atomic spacing between the amino cation and the phosphonate group permits simultaneous favorable inhibitor interactions with magnesium pyrophosphate and the 5′-phosphate binding site. The 5′-phosphonate of **3** interacts with neighboring residues similarly to the phosphate of ImmHP bound to *Pf*HGXPRT (PDB ID: 1CJB). The side chain residues of Tyr116 (2.6 Å), Thr149 (3.0 Å) and Thr152 (2.6 Å) and amides of Asp148 (3.1 Å), Thr149 (3.1 Å), Gly150 (2.6 Å) and Thr152 (2.9 Å) are in hydrogen bond distance with the 5′-phosphonate while the 3′-hydroxyl group of **3** forms a hydrogen bond with the side chain of Asp145 (2.8 Å). As **3** has only one hydroxyl group compared to two in the ribosyl transition state, a water molecule replaces the second hydroxyl group and forms a hydrogen bond network with the O2 and O4 of pyrophosphate (2.6 Å and 2.7 Å), the 3′-hydroxyl group (2.9 Å) and the cationic amine (2.9 Å). The single magnesium is chelated by Asp204,

three water molecules and pyrophosphate. Pyrophosphate forms hydrogen bonds with the side chains of Arg112 (2.9 Å) and Arg210 (2.8 Å) and the amides of Gly78 (3.0 Å), Lys77 (2.9 Å), Ser115 (2.9 Å) and Tyr116 (2.9 Å).

Binding of hypoxanthine to PfHGXPRT—Hypoxanthine is the physiologic substrate of the *Pf*HGXPRT reaction. Ligands in the complex of *Pf*HGXPRT with hypoxanthine and magnesium pyrophosphate interact with neighboring residues similar to those for ImmHP binding, except for the second magnesium (Fig. S2a). Although the hypoxanthine maintains a similar hydrogen bond network to bound ImmHP, hypoxanthine tilts 5° toward Phe197, an aromatic ring stacking interaction (Fig. S2b). The second magnesium in the *Pf*HGXPRT complex with hypoxanthine moves toward the 5′-phosphate binding site and is chelated to O1 of phosphate, the O2 of the pyrophosphate and four water molecules. Two water molecules form hydrogen bonds to Glu144 and Asp145 independently. Another water forms hydrogen bonds to N9 (2.6 Å) and O1 of the pyrophosphate (2.9 Å) and is positioned near the anomeric carbon position expected for the transition state.

Discussion

The transition state structures of other N-ribosyltransferases (Kline and Schramm, 1993; Lewandowicz and Schramm, 2004; Tao et al., 1996; Zhang et al., 2009) suggest a transition state for *Pf*HGXPRT that proceeds through an ribocation with a protonated purine leaving group (Fig. 1a) (Li et al., 1999). Immucillin-H 5′-phosphate resembles an early ribocationic transition state for *Pf*HGXPRT and is a nanomolar inhibitor of human and *P. falciparum* HG(X)PRTs. However, our results with **1** demonstrate that the 5′-phosphate group renders these potent inhibitors impermeable and/or makes them susceptible to phosphohydrolases inside cells.

The phosphonate group of the AIPs mimics phosphate, but is resistant to phosphohydrolases. Other phosphonates are in clinical use as antivirals [8]. Keough *et al* synthesized neutral 6-oxopurine ANPs that were able to inhibit recombinant *Pf*HGXPRT and demonstrate anti-malarial activity in *in vitro* culture (Keough et al., 2009). These substrate analogues validate *Pf*HGXPRT as an *in vitro* anti-malarial target. Our present advance is to develop mimics of the transition state with intrinsic binding affinity orders of magnitude tighter than neutral 6-oxopurine ANPs and with higher specificity for parasite relative to the human enzyme.

Adapting aminocations into the inhibitor scaffold incorporates transition state mimicry into these molecules. These molecules are synthetically accessible and are more biologically stable than ImmHP. The crystal structure of *Pf*HGXPRT bound to ImmHP and MgPP_i shows the ribosyl-mimic 2′- and 3′-hydroxl groups of ImmHP forming hydrogen bonds with Glu144, Asp145 and a water molecule coordinated by magnesium. Loss of these interactions might be expected to decrease the affinity of the AIPs, however this is not the case. The crystal structure of *Pf*HGXPRT bound to **3** and PP_i shows a more favorable ionic bond between PP_i and the riboxocarbenium mimic. A water molecule replaces the missing 2′-hydroxyl group. These structural changes allow the AIPs to adopt a favorable geometry in the catalytic site and account for their high affinity in spite of their structural simplicity. Additionally, the cationic reaction center of the AIPs creates favorable interactions that account for their significantly increased affinity for *Pf*HGXPRT as compared to the compounds presented by Keough *et al* with neutral reaction centers.

Inhibition of human HGPRT by an inhibitor of *Pf*HGXRPT is best avoided since genetic defects causing loss of human HGPRT activity leads to gouty arthritis (Kelley et al., 1968) and complete loss of activity is the cause of Lesch-Nyhan syndrome, a debilitating

neurological disorder (Lesch and Nyhan, 1964; Seegmiller et al., 1967). A selective inhibitor would avoid this potential problem and would also avoid increases in serum hypoxanthine levels by maintaining host HGPRT activity. Thus the ~500-fold selectivity for *Pf*HGXPRT demonstrated by **2** and **3** (Fig. 1c) is beneficial.

Phosphonate groups have two negative charges at physiologic pH and are slowly taken up by human cells via endocytosis (Connelly et al., 1993). Neither **2** nor **3** demonstrated activity against cultured parasites, likely due to poor cell permeability. To target *Pf*HGXPRT, prodrugs of **2** or **3** must enter the erythrocyte and cross the parasitophorous vacuole and the parasite plasma membranes. Compound **4**, the bis-pivalate prodrug of **2**, is able to cross into the erythrocyte. However, our data suggest it is rapidly metabolized in the erythrocyte to form **2** which inhibits erythrocyte PNP and is unable to permeate the parasite cytoplasm.

A prodrug strategy that has been used to increase the efficacy of the nucleoside phosphonates cidofovir and tenofovir was more successful (Hostetler, 2009). The lysophospholipid tail allows for transfer through cellular membranes. Inside target cells, phospholipase C (PLC) activity cleaves the prodrug releasing the acyclic phosphonate inhibitor. This system is advantageous for targeting *P. falciparum* since the Ca^{2+}-dependent PLC activity in erythrocytes displays a narrow substrate specificity for phosphorylated phosphoinositides and a PLC with broad substrate specificity has been identified in *P. falciparum* (Allan and Michell, 1978; Ferrell and Huestis, 1984; Hanada et al., 2000; Hanada et al., 2002). In lysophospholipid prodrugs of **2**, phosphocholine is replaced by an AIP, the sn2 hydroxyl is replaced with a hydrogen and the sn3 ester linkage is replaced with an ether. This creates prodrugs with activity against cultured *P. falciparum.* Inhibition of hypoxanthine incorporation into parasite nucleotide pools establishes *Pf*HGXPRT as the target.

Following cellular activation, **2** is sequestered inside the parasites. In metabolic labeling experiments effective inhibition of *Pf*HGXPRT remained even when excess prodrug was removed. The difference between the K_i of **2** (10 nM) and the IC_{50} of its prodrugs (~3 μM) indicate that further optimization of the prodrug scaffold is needed in the future.

Crystal structures of *Pf*HGXPRT with **3** or hypoxanthine show similar active sites to that of *Pf*HGXPRT in complex with ImmHP and also to *Hs*HGPRT in complex with Immucillin-GP (PDB ID: 1CJB and 1BZY) (Shi et al., 1999a; Shi et al., 1999b). In all structures the catalytic loop of the hood domain is closed over the active site and all residues in the active site overlap closely. The structural similarity suggests the selectivity of the AIPs for *Pf*HGXPRT arise from more favorable interactions of the ion pair between inhibitor and bound magnesium pyrophosphate.

The structure of *Pf*HGXPRT bound to **3**, magnesium and pyrophosphate reveals the structural basis of the high affinity binding. Structures of *Pf*HGXPRT and *Hs*HGPRT show similar positioning of three elements, purine base, 5′-phosphate and pyrophosphate, regardless of transition state mimicry. This geometry establishes a six-bond distance between the nucleobase and the phosphorous atom as the favored catalytic site spacing. The acyclic structure of **3** maintains this distance while establishing a 2.8 Å ion pair between the amino cation and O1 of pyrophosphate. Crystal structures of *Pf*HGXPRT with ImmHP show a 3.2 Å ion pair. The stereochemistry of **3** places the amino cation for favorable ion pair formation and tight binding, even though some contacts of the ribosyl group are missing. The truncated structure of **3** allows an additional water molecule into the active site, replacing the 2′-hydroxyl of ImmHP in the hydrogen bond network. The decreased ion-pair

distance and the structural water compensate energetically for the loss of the 2′-hydroxyl of ImmHP giving **3** an inhibition constant similar to ImmHP.

A detailed kinetic mechanism of *Pf*HGXPRT has not yet been described, however the mechanisms of other HG(X)PRTs follow an ordered sequential mechanism with PRPP binding first, followed by purine base binding (Munagala et al., 1998; Wenck et al., 2004; Xu et al., 1997). This mechanism predicts a dead-end complex formed by the purine base and pyrophosphate. The crystal structure of *Pf*HGXPRT, hypoxanthine and magnesium is the first structural validation of this complex.

Significance

The AIPs and their lysophospholipid prodrugs represent an advance in the development of *Pf*HGXPRT inhibitors as potential anti-malarial compounds. The AIPs are able to match the affinity of ImmHP, are able to resist the action of phosphohydrolases, are highly selective for the parasite enzyme and show improved characteristics for synthesis. The lysophospholipid prodrugs of the AIPs demonstrate activity against cultured *P. falciparum* and robustly inhibit the incorporation of hypoxanthine into the parasite nucleotide pool. This evidence extends the work of Keough *et al.* and provides additional metabolic validation of *Pf*HGXPRT as an *in vitro* antimalarial target.

Experimental Procedures

Gene construction and protein purification

codon-optimized genes were obtained from DNA 2.0 (Menlo Park, CA) using the amino acid sequence from *Pf*HGXPRT (Gene ID: PF10_0121, http://plasmodb.org/plasmo) and the human HGPRT crystal structure (Protein Data Bank ID: 1BZY). An N-terminal thrombin cleavable 6-His tag (MGSSHHHHHHSSGLVPNGSH) was added to aid in purification. The gene was inserted in pDONR221 (Invitrogen). Both plasmids were overexpressed in BL21AI cells and enzymes were purified by methods described previously (Taylor et al., 2007b). *Pf*HGXPRT was dialysed against 50 mM potassium phosphate pH 7.5, 150 mM KCl, 5 mM imidazole, 1 mM DTT and 10% glycerol and human HGPRT against 10 mM Tris pH 7.5, 150 mM KCl, 5 mM imidazole, 1 mM DTT and 10% glycerol. The enzymes were then concentrated to ~15 mg ml^{-1} and frozen drop-wise in liquid nitrogen. PNP was purified as previously described (Taylor et al., 2007a).

Inhibitors and prodrugs

Compounds **1–8** were synthesized at Industrial Research Limited, Lower Hutt, New Zealand and detailed synthetic procedures will be published separately.

Inhibition assays

*Pf*HGXPRT activity was measured using spectrophotometric assays observing the conversion of xanthine and 5-phospho-α-D-ribose-1-pyrophosphate to xanthosine-5′-monophosphate and inorganic pyrophosphate (PP$_i$) at 247 nm (ε_{257} – 6.8 mM^{-1}cm^{-1}) or the conversion of guanine and PRPP to guanosine-5′-monophosphate and PP$_i$ (ε_{257} – 5.8 mM^{-1}cm^{-1}) on a Varian Cary 100 spectrophotometer (Palo Alto, CA) at 37 °C. All assays were conducted in 10 mM potassium phosphate, pH 7.6, 10 mM MgCl$_2$, 1 mM PRPP, 150 μM xanthine or 50 μM guanine, 0.5 mM DTT with varying amounts of inhibitor and concentrations of *Pf*HGXPRT between 2 and 10 nM or human HGPRT of 1 nM. As the dissociation constants of many of the inhibitors were near or below that of the enzyme concentration, the data were fit to the Morrison equation for tight-binding inhibitors

(Morrison, 1969). PNP inhibition assays were carried out as previously described (Clinch et al., 2009).

Crystallization, Data Collection, and Structural Determination

*Pf*HGXPRT was concentrated to 12– 20 mg ml^{-1} and dialyzed with either 50 mM phosphate buffer at pH 7.4 or 50 mM NaCl and 10 mM Tris buffer at pH 7.4. Prior to protein crystallization, *Pf*HGXPRT was incubated on ice with 1 mM hypoxanthine, 2 mM PP$_i$ and 5 mM MgCl$_2$ or 1 mM **3**, 2 mM PP$_i$ and 2 mM MgCl$_2$. The hypoxanthine-bound *Pf*HGXPRT was crystallized in 20% PEG3350, 0.2 M sodium citrate and the complex of *Pf*HGXPRT with **3** was crystallized in 20% PEG3350, 0.2 M ammonium citrate at pH 7.0 using the sitting drop vapor diffusion method at 18 °C. Crystals were briefly transferred to the reservoir solution supplemented with 20% glycerol and frozen in liquid N$_2$ before data collection.

X-ray diffraction data was collected at beamline X29A of Brookhaven National Laboratory on an ADSC Q315 detector at 100 K. Data was processed with the HKL2000 program suite and data processing statistics are provided in Table 2 (Otwinowski and Minor, 1997).

The crystal structures of liganded *Pf*HGXPRT were determined by molecular replacement in Molrep using the published structure of *Pf*HGXPRT from which ImmHP, PP$_i$, Mg^{2+} ion and water molecules were removed as the search model (PDB ID: 1CBJ) (CCP, 1994). The model without ligands was first rebuilt in COOT and refined in Refmac5 (Emsley and Cowtan, 2004; Potterton et al., 2003). The ligands were later included in COOT using the F_o - F_c map when the R$_{free}$ was below 30% and further refined in Refmac5. A phosphate ion was found in the active site of *Pf*HGXPRT in complex with hypoxanthine and magnesium pyrophosphate based on the strong positive peak in the F_o - F_c electron density map. The final model was validated by Molprobity. The refinement statistics are summarized in Table 2. The coordinates and structure factors for the hypoxanthine- and C-complexes of *Pf*HGXPRT were deposited in the Protein Data Bank under accession codes 3OZG and 3OZF, respectively.

Cell culture inhibition assay

Activity of compounds were tested as previously described (Cassera et al., 2008). Compounds **5** and **6** were dissolved in sterile water by sonication in a warm water bath; compound **7** was dissolved in DMSO; compound **8** was poorly soluble in water or DMSO. Compound **8** was dissolved in sterile water, added to malaria culture media and concentrated by lyphophilization.

Metabolic labeling

Erythrocytes, infected erythrocytes and erythrocyte-free parasites in the trophozoite stage were treated with 25 μM **1**, 100 μM **4**, 10 μM **5** and **6** or 15 μM **8** for one hour at 37 °C. Cells were then labeled with 1 μM [2,8-^{3}H]hypoxanthine (30 Ci/mmol, Moravek) or 1 μM [2,8-^{3}H]inosine (50 Ci/mmol, Moravek) for 1 hour at 37 °C. Parasites from infected erythrocytes were isolated by lysis with 0.045% saponin either before addition of radiolabel or after incubation with radiolabel. Proteins and nucleic acids were removed by perchloric acid treatment of supernatants and cell pellets (Cassera et al., 2008). All samples were analyzed by HPLC with a modification in the previously described solvent gradient (Cassera et al., 2008). Briefly, the mobile phases were 8 mM tetrabutylammonium bisulfate (Fluka) and 100 mM KH$_2$PO$_4$ with the pH adjusted to 6.0 with KOH in water (solution A) or 30% acetonitrile (solution B). The HPLC gradient was from 0% to 10% solution B in 4 min and maintained for 2 min, 10% to 20% solution B in 1 min, 20% to 40% solution B in 10 min, 40% to 100% solution B in 3 min and maintained for 4 min.

UPLC/MS/MS

Samples were placed in 96 deep-well plates, treated with 0.5 M $HClO_4$ at 1:7 (v/v, sample/ $HClO_4$), incubated for 20 min at 4 °C and neutralized with 5 M KOH at 10:1 (v/v, $HClO_4$/ KOH) for 20 min at 4 °C. Plates were centrifuged (10 min at 4,000 rpm, 4 °C) and supernatants were filtered through a MultiScreen® Filter Plate with Ultracel®-10 Membrane (Millipore). Metabolite and inhibitor levels were analyzed by UPLC/MS/MS using a Xevo TQD mass spectrometer (Waters). The separation of inosine, hypoxanthine, and inhibitors was achieved with an Acquity HSS T3 column (2.1×100 mm, 1.8 μm, Waters) at 60 °C. The eluent system was composed of 5 mM ammonium formate in water (A) and 5 mM ammonium formate in methanol (B) with a gradient of 98% eluent A to 30% eluent B from 0.1 to 1 min, 70% eluent A to 80% eluent B from 1 to 1.5 min and back to 98% eluent A from 1.5 to 3 min at a flow rate of 0.6 ml min^{-1}. Detection was performed in ESI positive-ion mode using multiple-reaction monitoring (MRM) mode. For ESI-MS/MS analysis, the following ion transitions, cone voltage (CV) and collision energy (CE) were used: inosine m/z 269.1 >137.1 (CV: 14 V, CE: 12 eV), hypoxanthine m/z 137.1 >110.0 (CV: 42 V, CE: 18 eV), compound **1** m/z 659.06 >212.90 (CV: 34 V, CE: 40 eV), compound **2** m/z 286.92 >139.74 (CV: 22 V, CE: 14 eV), compound **4** m/z 515.05 >205.76 (CV: 34 V, CE: 28 eV). The ESI capillary voltage was 0.3 kV, source temperature was set at 150 °C and desolvation temperature at 450 °C. Data acquisition and analysis were carried out by MassLynx V4.1 and QuanLynx software.

Supplementary Material

Refer to Web version on PubMed Central for supplementary material.

Acknowledgments

References

Allan D, Michell RH. A calcium-activated polyphosphoinositide phosphodiesterase in the plasma membrane of human and rabbit erythrocytes. Biochim Biophys Acta. 1978; 508:277–286. [PubMed: 205246]

Bejon P, Lusingu J, Olotu A, Leach A, Lievens M, Vekemans J, Mshamu S, Lang T, Gould J, Dubois MC, et al. Efficacy of RTS,S/AS01E vaccine against malaria in children 5 to 17 months of age. N Engl J Med. 2008; 359:2521–2532. [PubMed: 19064627]

Berman PA, Human L. Hypoxanthine depletion induced by xanthine oxidase inhibits malaria parasite growth in vitro. Adv Exp Med Biol. 1991; 309A:165–168. [PubMed: 1789199]

Cassera MB, Hazleton KZ, Merino EF, Obaldia N 3rd, Ho MC, Murkin AS, DePinto R, Gutierrez JA, Almo SC, Evans GB, et al. Plasmodium falciparum parasites are killed by a transition state analogue of purine nucleoside phosphorylase in a primate animal model. PloS One. 2011; 6:e26916. [PubMed: 22096507]

Cassera MB, Hazleton KZ, Riegelhaupt PM, Merino EF, Luo M, Akabas MH, Schramm VL. Erythrocytic adenosine monophosphate as an alternative purine source in Plasmodium falciparum. J Biol Chem. 2008; 283:32889–32899. [PubMed: 18799466]

Clinch K, Evans GB, Frohlich RF, Furneaux RH, Kelly PM, Legentil L, Murkin AS, Li L, Schramm VL, Tyler PC, et al. Third-generation immucillins: syntheses and bioactivities of acyclic immucillin inhibitors of human purine nucleoside phosphorylase. Journal of medicinal chemistry. 2009; 52:1126–1143. [PubMed: 19170524]

Collaborative Computing Project. The CCP4 suite: programs for protein crystallography. Acta Crystallogr D Biol Crystallogr. 1994; 50:760–763. [PubMed: 15299374]

Connelly MC, Robbins BL, Fridland A. Mechanism of uptake of the phosphonate analog (S)-1-(3-hydroxy-2-phosphonylmethoxypropyl)cytosine (HPMPC) in Vero cells. Biochem Pharmacol. 1993; 46:1053–1057. [PubMed: 8216348]

Emsley P, Cowtan K. Coot: model-building tools for molecular graphics. Acta Crystallogr D Biol Crystallogr. 2004; 60:2126–2132. [PubMed: 15572765]

Ferrell JE, Huestis WH. Phosphoinositide metabolism and the morphology of human erythrocytes. J Cell Biol. 1984; 98:1992–1998. [PubMed: 6327723]

Hanada K, Mitamura T, Fukasawa M, Magistrado PA, Horii T, Nishijima M. Neutral sphingomyelinase activity dependent on Mg2+ and anionic phospholipids in the intraerythrocytic malaria parasite Plasmodium falciparum. The Biochemical journal. 2000; 346(Pt 3):671–677. [PubMed: 10698693]

Hanada K, Palacpac NM, Magistrado PA, Kurokawa K, Rai G, Sakata D, Hara T, Horii T, Nishijima M, Mitamura T. Plasmodium falciparum phospholipase C hydrolyzing sphingomyelin and lysocholinephospholipids is a possible target for malaria chemotherapy. The Journal of experimental medicine. 2002; 195:23–34. [PubMed: 11781362]

Hostetler KY. Alkoxyalkyl prodrugs of acyclic nucleoside phosphonates enhance oral antiviral activity and reduce toxicity: current state of the art. Antiviral Res. 2009; 82:A84–A98. [PubMed: 19425198]

Kelley WN, Rosenbloom FM, Miller J, Seegmiller JE. An enzymatic basis for variation in response to allopurinol. Hypoxanthine-guanine phosphoribosyltransferase deficiency. N Engl J Med. 1968; 278:287–293. [PubMed: 5638346]

Keough DT, Hockova D, Holy A, Naesens LM, Skinner-Adams TS, Jersey J, Guddat LW. Inhibition of hypoxanthine-guanine phosphoribosyltransferase by acyclic nucleoside phosphonates: a new class of antimalarial therapeutics. J Med Chem. 2009; 52:4391–4399. [PubMed: 19527031]

Kicska GA, Tyler PC, Evans GB, Furneaux RH, Kim K, Schramm VL. Transition state analogue inhibitors of purine nucleoside phosphorylase from Plasmodium falciparum. J Biol Chem. 2002a; 277:3219–3225. [PubMed: 11707439]

Kicska GA, Tyler PC, Evans GB, Furneaux RH, Schramm VL, Kim K. Purine-less death in Plasmodium falciparum induced by immucillin-H, a transition state analogue of purine nucleoside phosphorylase. J Biol Chem. 2002b; 277:3226–3231. [PubMed: 11706018]

Kline PC, Schramm VL. Purine nucleoside phosphorylase. Catalytic mechanism and transition-state analysis of the arsenolysis reaction. Biochemistry. 1993; 32:13212–13219. [PubMed: 8241176]

Kline PC, Schramm VL. Pre-steady-state transition-state analysis of the hydrolytic reaction catalyzed by purine nucleoside phosphorylase. Biochemistry. 1995; 34:1153–1162. [PubMed: 7827065]

Lesch M, Nyhan WL. A Familial Disorder of Uric Acid Metabolism and Central Nervous System Function. Am J Med. 1964; 36:561–570. [PubMed: 14142409]

Lewandowicz A, Schramm VL. Transition state analysis for human and Plasmodium falciparum purine nucleoside phosphorylases. Biochemistry. 2004; 43:1458–1468. [PubMed: 14769022]

Li CM, Tyler PC, Furneaux RH, Kicska G, Xu Y, Grubmeyer C, Girvin ME, Schramm VL. Transition-state analogs as inhibitors of human and malarial hypoxanthine-guanine phosphoribosyltransferases. Nat Struct Biol. 1999; 6:582–587. [PubMed: 10360365]

Morrison JF. Kinetics of the reversible inhibition of enzyme-catalysed reactions by tight-binding inhibitors. Biochim Biophys Acta. 1969; 185:269–286. [PubMed: 4980133]

Munagala NR, Chin MS, Wang CC. Steady-state kinetics of the hypoxanthine-guanine-xanthine phosphoribosyltransferase from Tritrichomonas foetus: the role of threonine-47. Biochemistry. 1998; 37:4045–4051. [PubMed: 9521725]

Noedl H, Se Y, Schaecher K, Smith BL, Socheat D, Fukuda MM. Evidence of artemisinin-resistant malaria in western Cambodia. N Engl J Med. 2008; 359:2619–2620. [PubMed: 19064625]

Otwinowski, Z.; Minor, W. Carter, Charles W, Jr. Methods in Enzymology. Academic Press; 1997. [20] Processing of X-ray diffraction data collected in oscillation mode; p. 307-326.

Potterton E, Briggs P, Turkenburg M, Dodson E. A graphical user interface to the CCP4 program suite. Acta Crystallogr D Biol Crystallogr. 2003; 59:1131–1137. [PubMed: 12832755]

Reyes P, Rathod PK, Sanchez DJ, Mrema JE, Rieckmann KH, Heidrich HG. Enzymes of purine and pyrimidine metabolism from the human malaria parasite, Plasmodium falciparum. Mol Biochem Parasitol. 1982; 5:275–290. [PubMed: 6285190]

Seegmiller JE, Rosenbloom FM, Kelley WN. Enzyme defect associated with a sex-linked human neurological disorder and excessive purine synthesis. Science. 1967; 155:1682–1684. [PubMed: 6020292]

Shi W, Li CM, Tyler PC, Furneaux RH, Cahill SM, Girvin ME, Grubmeyer C, Schramm VL, Almo SC. The 2.0 A structure of malarial purine phosphoribosyltransferase in complex with a transition-state analogue inhibitor. Biochemistry. 1999a; 38:9872–9880. [PubMed: 10433693]

Shi W, Li CM, Tyler PC, Furneaux RH, Grubmeyer C, Schramm VL, Almo SC. The 2.0 A structure of human hypoxanthine-guanine phosphoribosyltransferase in complex with a transition-state analog inhibitor. Nat Struct Biol. 1999b; 6:588–593. [PubMed: 10360366]

Tao W, Grubmeyer C, Blanchard JS. Transition state structure of Salmonella typhimurium orotate phosphoribosyltransferase. Biochemistry. 1996; 35:14–21. [PubMed: 8555167]

Taylor EA, Clinch K, Kelly PM, Li L, Evans GB, Tyler PC, Schramm VL. Acyclic ribooxacarbenium ion mimics as transition state analogues of human and malarial purine nucleoside phosphorylases. J Am Chem Soc. 2007a; 129:6984–6985. [PubMed: 17497780]

Taylor EA, Rinaldo-Matthis A, Li L, Ghanem M, Hazleton KZ, Cassera MB, Almo SC, Schramm VL. Anopheles gambiae purine nucleoside phosphorylase: catalysis, structure, and inhibition. Biochemistry. 2007b; 46:12405–12415. [PubMed: 17918964]

Wenck MA, Medrano FJ, Eakin AE, Craig SP. Steady-state kinetics of the hypoxanthine phosphoribosyltransferase from Trypanosoma cruzi. Biochim Biophys Acta. 2004; 1700:11–18. [PubMed: 15210120]

World Health Organization. Geneva: 2008. World Malaria Report.

Xu Y, Eads J, Sacchettini JC, Grubmeyer C. Kinetic mechanism of human hypoxanthine-guanine phosphoribosyltransferase: rapid phosphoribosyl transfer chemistry. Biochemistry. 1997; 36:3700–3712. [PubMed: 9132023]

Zhang Y, Luo M, Schramm VL. Transition states of Plasmodium falciparum and human orotate phosphoribosyltransferases. J Am Chem Soc. 2009; 131:4685–4694. [PubMed: 19292447]

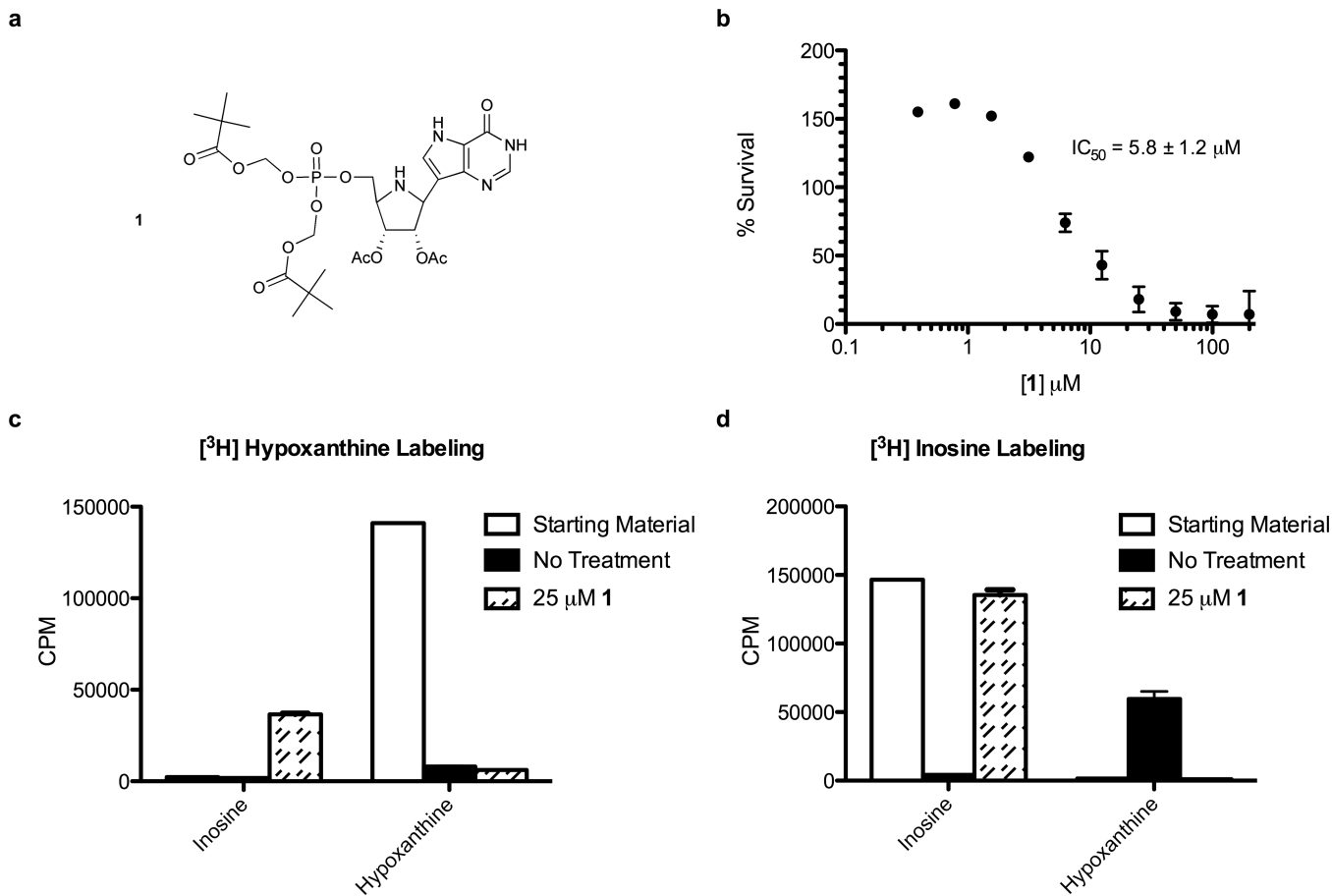## Highlights

- *P. falciparum* are purine auxotrophs and HGXPRT is an essential enzyme

- Transition state analogues of HGXPRT are powerful enzyme inhibitors

- Blocking HGXPRT action kills *P. falciparum* in infected erythrocytes

- Prodrugs of HGXPRT transition state analogues are biologically available
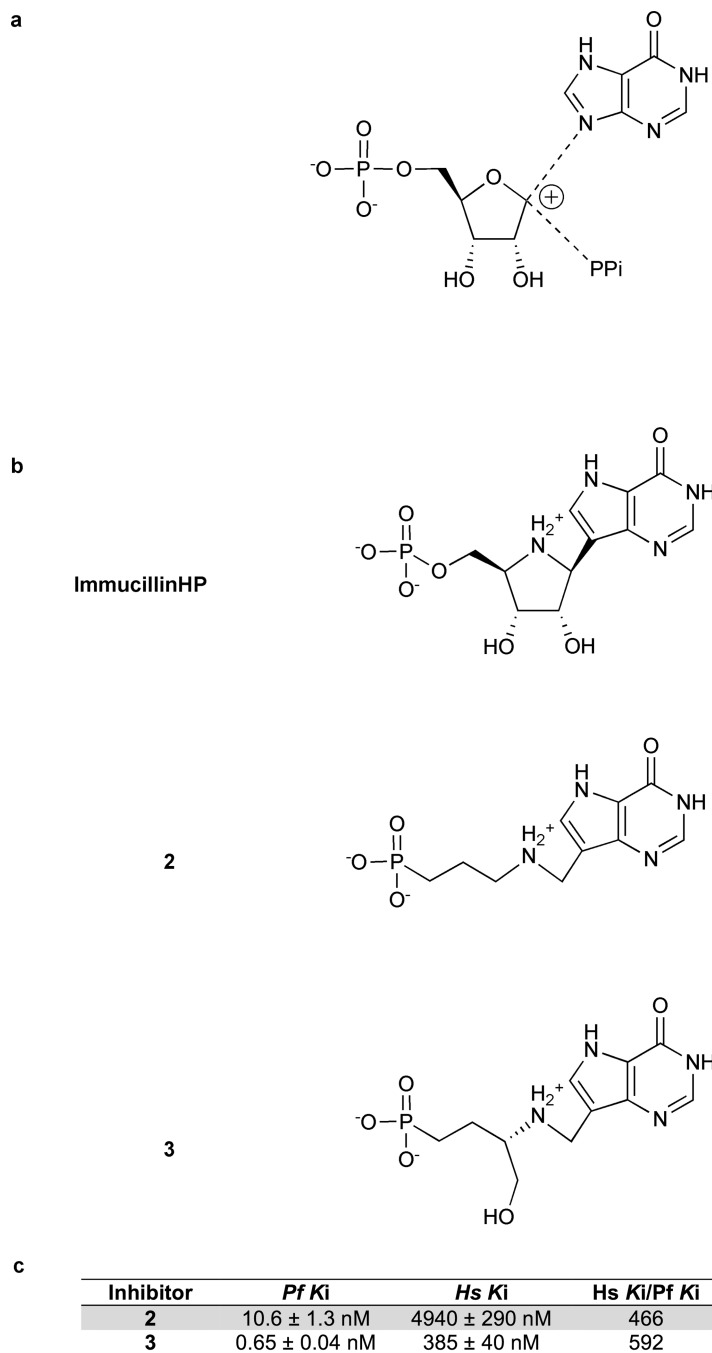
Figure 1. Proposed HGXPRT transition state structures and transition state analogs of *Pf*HGXPRT

(a) Proposed transition state based on the transition states of enzymes catalyzing similar reactions. Li *et al* (1999) proposed this transition state for HG(X)PRT with a protonated N7 and oxocarbenium ion formation at C1′. (b) Immucillin-H 5′-phosphate was designed as a mimic of this proposed transition state. The acyclic Immucillin phosphonates (AIPs) **2** and **3** are powerful and selective inhibitors of *Pf*HGXPRT. The AIPs maintain key features of Immucillin-H 5'-phosphate including the 9-deazahypoxanthine nucleobase, ribocationic nitrogen, and a phosphonate group. (c) The inhibition constants for **2** and **3** with *Pf*HGXPRT and human HGPRT.

a

1

b

$IC_{50} = 5.8 \pm 1.2 \ \mu M$

% Survival

[**1**] μM

c

[^{3}H] Hypoxanthine Labeling

CPM

☐ Starting Material
■ No Treatment
▨ 25 μM **1**

Inosine   Hypoxanthine

d

[^{3}H] Inosine Labeling

CPM

☐ Starting Material
■ No Treatment
▨ 25 μM **1**

Inosine   Hypoxanthine

Figure 2. A prodrug of Immucillin-H 5'-phosphate (ImmHP) is converted to Immucillin-H by intracellular activities

(a) The structure of ImmHP bis-pivalate prodrug **1**. (b) Inhibition of cultured parasite growth by **1**. (c) Extracellular purine analysis of metabolic labeling with [^{3}H]hypoxanthine in uninfected erythrocytes treated with 25 μM **1**. (d) The same experiment as in (c) but labeling with [^{3}H]inosine. See also Table S1.

a

4

b

$IC_{50} = 45 \pm 6$ μM

[4] μM

c

[³H] Hypoxanthine Labeling

Starting Material
No Treatment
100 μM **4**

CPM

Inosine   Hypoxanthine

d

[³H] Inosine Labeling

Starting Material
No Treatment
100 μM Compound **8**

CPM

Inosine   Hypoxanthine

Figure 3. Acyclic Immucillin phosphonate (AIP) prodrugs must avoid activation in the erythrocyte to reach parasite targets

(a) The structure of AIP prodrug **4**, the bispivalate compound prodrug of **2**. (b) Inhibition of parasite growth inhibition by **4**. (c) Extracellular purine analysis of metabolic labeling in uninfected erythrocytes treated with 100 μM **1** and [³H]hypoxanthine. (d) The same experimental design as in (c) but labeling with [³H]inosine. See also Table S2.

a

Cleavage of lysophosphatidylcholine
by phospholipases

b

Proposed cleavage of alkoxyalkyl Immucillin
prodrugs by phospholipases

| R_1	R_2	Compound	Strain	IC50 (μM)
$(CH_2)_{16}CH_3$	Et	**5**	3D7	2.5 ± 0.2
			Dd2	3.0 ± 0.1
			FVO	2.9 ± 0.1
$(CH_2)_{14}CH_3$	Et	**6**	3D7	1.9 ± 0.1
			Dd2	2.3 ± 0.1
			FVO	3.1 ± 0.1
$(CH_2)_{16}CH_3$	H	**7**	3D7	7.0 ± 0.1
$(CH_2)_{16}CH_3$	$(CH_2)_{16}CH_3$	**8**	3D7	> 15

c
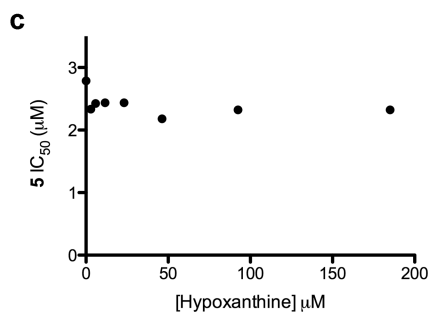
Figure 4. Lysophospholipid prodrugs increase the biological activity of the AIPs
The prodrug approach summarized by Hostetler (Hostetler, 2009) was adapted to the AIPs.
(a) and (b) are schematic representation of the AIP prodrugs and the IC$_{50}$ values of
compounds **5** to **8**. (c) The biological IC$_{50}$ values of **5** conducted at varying exogenous
hypoxanthine concentrations.
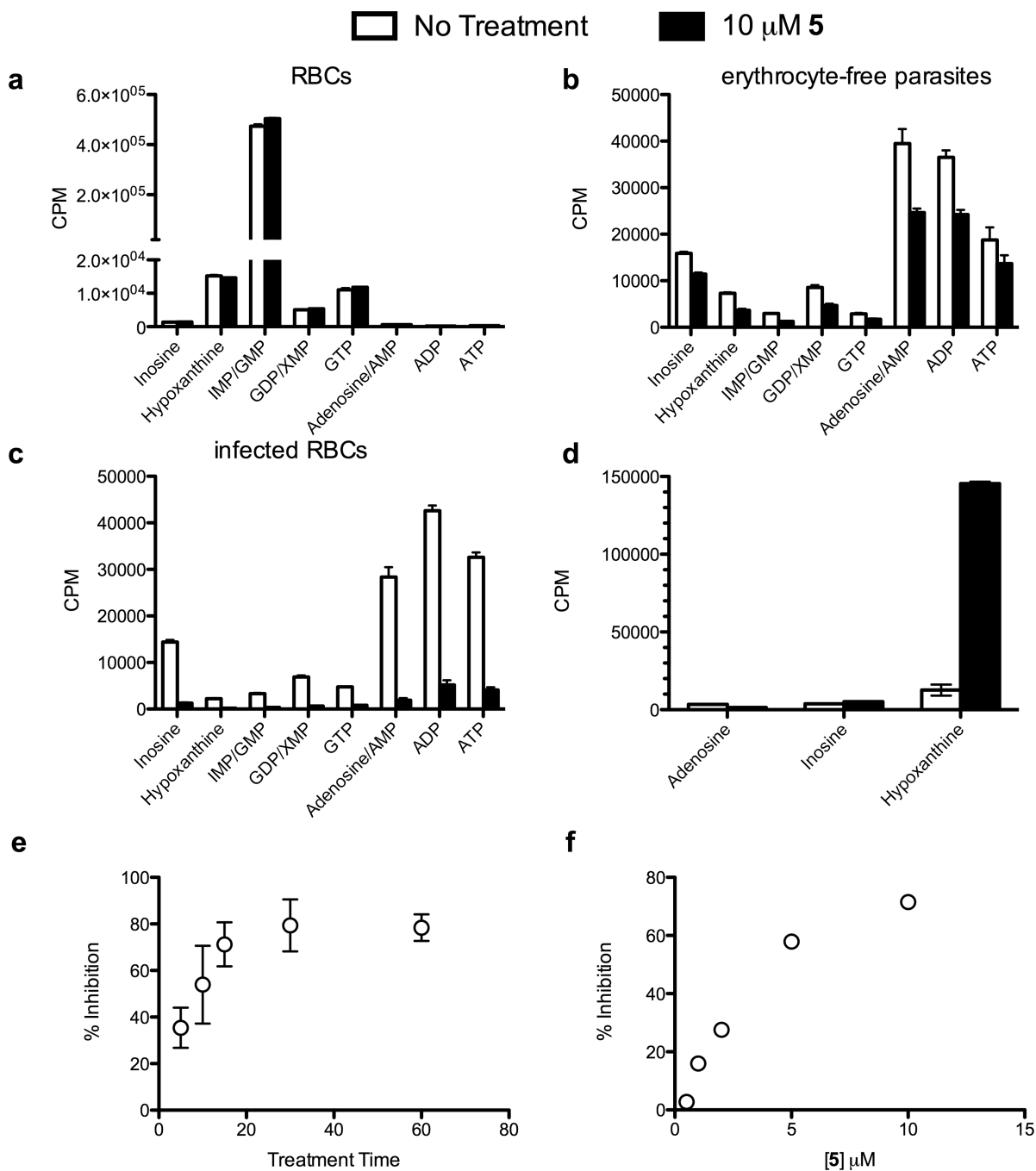
Figure 5. Treatment of infected RBCs with AIP prodrugs inhibits *Pf*HGXPRT
Cells were metabolically labeled with [2,8-^{3}H]hypoxanthine in the presence or absence of
10 μM **5** by incubation as in the methods. Purine incorporation was quantitated by HPLC of
(a) uninfected RBCs, (b) erythrocyte-free parasites, (c) parasites isolated from infected
erythrocytes, (d) extracellular purines from panel (c). The time (e) and concentration (f)
dependence of label uptake were measured by liquid scintillation counting of spent media.
The results are summarized in Table 1. See also Figure S1.
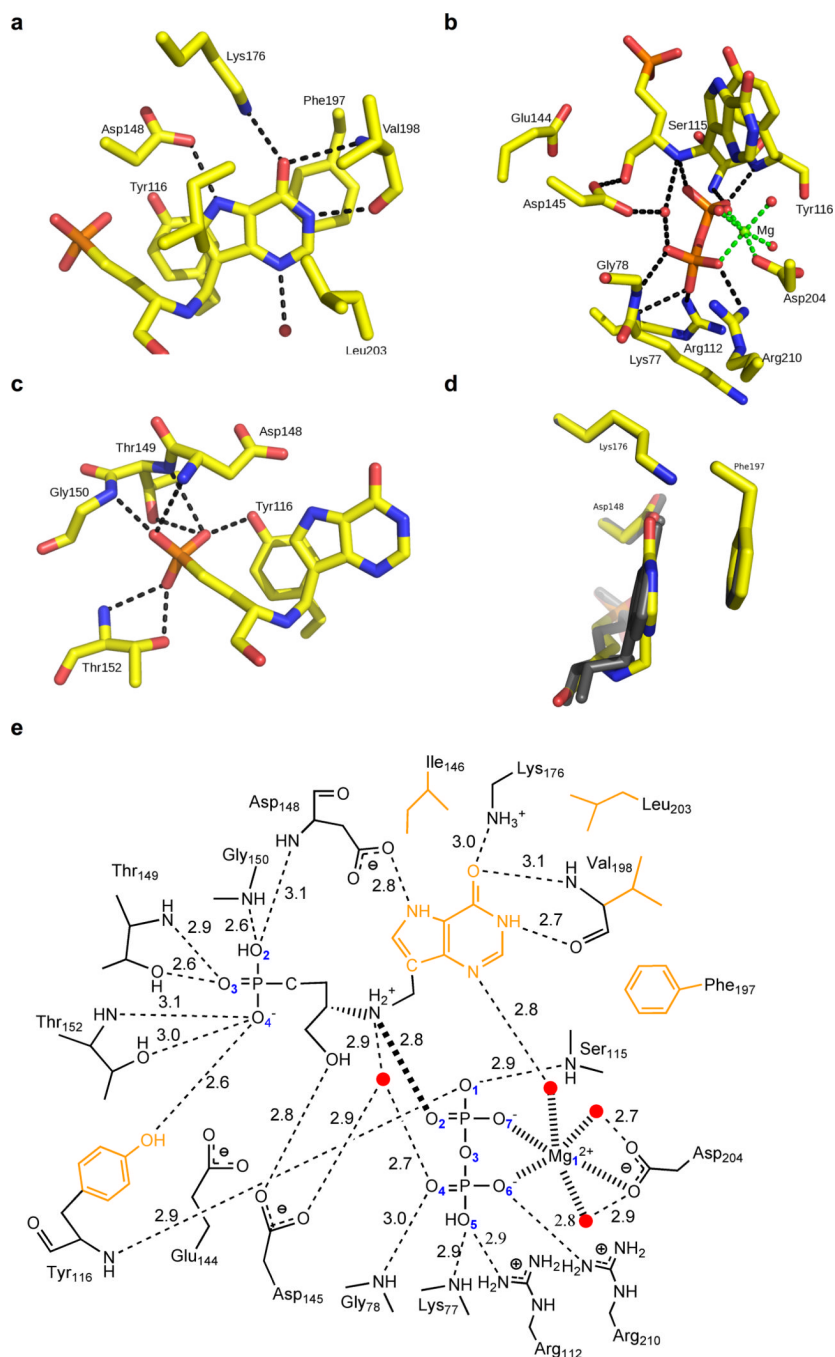
Figure 6. The active site of *Pf*HGXPRT bound to AIP-3 and MgPP$_i$
Hydrogen bonds are represented as dashed lines. (a) The purine binding site. (b) The pyrophosphate and ribose binding sites with the ionic bonds coordinating magnesium represented as green dashed lines. (c) The 5′-phosphate binding site. (d) Comparison of the purine nucleobase positions of ImmHP and **3** illustrating the 11° tilt of nucleobase **3** compared to ImmHP. (e) Two-dimensional representation of the active site where the ionic bond between pyrophosphate and the ribocation mimic is represented as a thick dashed line. Water molecules are represented as red dots and the hydrophobic residues interacting with the purine ring are drawn in orange. See also Figure S2.

Table 1

Metabolic labeling summary showing the percentage change in incorporation of radiolabel from [2, 8-^{3}H]hypoxanthine into the nucleotide pool of *P. falciparum* observed with treatment of 10 μM **5**.

Metabolite	Labeling Condition		
	RBCs	Free Parasites	Infected RBCs
Inosine	2 ± 5	-38 ± 22	-84 ± 8
Hypoxanthine	-4 ± 1	-40 ± 50	-88 ± 3
IMP/GMP	6 ± 1	-55 ± 26	-88 ± 3
GDP/XMP	5 ± 2	-44 ± 23	-88 ± 4
GTP	7 ± 1	-48 ± 19	-75 ± 9
Adenosine/AMP	-2 ± 1	-37 ± 31	-91 ± 3
ADP	-9 ± 4	-41 ± 20	-79 ± 11
ATP	-3 ± 3	-42 ± 22	-68 ± 22

Table 2

Crystallographic data collection and refinement statistics

	Hypoxanthine	3
PDB codes	**3OZF**	**3OZG**
Data collection		
Space group	$P2_1$	$C222_1$
Cell dimension		
a, b, c (Å)	75.0, 88.9, 80.4	105.1, 110.6, 173.3
α, β, γ (°)	90.0, 117.1, 120.0	90.0, 90.0, 90.0
Resolutions (Å)	50.00–1.95	20.00–2.00
	(2.02–1.95)	(2.07–2.00)
Rsym (%)	9.3 (41.3)	14.9 (70.7)
I / σI	15.1 (3.8)	12.5 (1.8)
Completeness (%)	99.9 (99.9)	98.5 (88.7)
Redundancy	4.9 (4.5)	7.3 (5.6)
Refinement		
Resolution (Å)	50.00–1.95	20.00–2.00
No. unique reflections	68875	67383
R_{work} / R_{free} (%)	18.9/23.7	21.9/26.4
B-factors (Å^2)		
Protein		
(*main chain*)	19.3	28.0
(*side chain*)	22.1	29.5
Water	25.3	28.1
Ligand	20.0	24.7
No. of Atoms		
Protein	7444	7390
Water	409	212
Ligand	102	124
R.m.s deviations		
Bond lengths (Å)	0.015	0.012
Bond angles (°)	1.53	1.50
Ramchadran analysis		
favored region	95.8%	96.0%
allowed region	4.2%	4.0%
disallowed region	0%	0%
Coordinate Error by Luzzati plot (Å)	0.21	0.28